CLIMATOLOGY

Disentangling the mechanisms of equatorial Pacific climate change

Sarah M. Kang[1]*, Yechul Shin[2]*, Hanjun Kim[3], Shang-Ping Xie[4], Shineng Hu[5]

Most state-of-art models project a reduced equatorial Pacific east-west temperature gradient and a weakened Walker circulation under global warming. However, the causes of this robust projection remain elusive. Here, we devise a series of slab ocean model experiments to diagnostically decompose the global warming response into the contributions from the direct carbon dioxide (CO_2) forcing, sea ice changes, and regional ocean heat uptake. The CO_2 forcing dominates the Walker circulation slowdown through enhancing the tropical tropospheric stability. Antarctic sea ice changes and local ocean heat release are the dominant drivers for reduced zonal temperature gradient over the equatorial Pacific, while the Southern Ocean heat uptake opposes this change. Corroborating our model experiments, multimodel analysis shows that the models with greater Southern Ocean heat uptake exhibit less reduction in the temperature gradient and less weakening of the Walker circulation. Therefore, constraining the tropical Pacific projection requires a better insight into Southern Ocean processes.

INTRODUCTION

Greenhouse gas–induced warming exhibits substantial spatial variations although the CO_2 radiative forcing is largely homogeneous in space (*1*). Changing sea surface temperature (SST) pattern over the equatorial Pacific is of particular importance as it drives pronounced changes in regional and global climate. For example, the spatial pattern of projected SST change controls the spatial pattern of rainfall changes in the tropical Pacific following the warmer-get-wetter mechanism (*2*, *3*). Accompanying shift in the location of deep convection is communicated into higher latitudes by Rossby waves (*4*). Moreover, changes in zonal gradient of equatorial Pacific SST can modulate the El Niño–Southern Oscillation flavor (*5*) and amplitude (*6*), which, in turn, is proposed to drive Southern Ocean warming (*7*). Specifically, an El Niño–like mean SST change is likely to generate more eastern Pacific El Niño events, increasing precipitation over North America (*8*). The tropical Pacific SST warming pattern also controls the global climate feedbacks associated with clouds and lapse rate, thereby exerting a critical impact on the magnitude of climate sensitivity (*9*–*12*).

A number of factors come into play for the pattern formation of greenhouse gas–induced tropical Pacific warming. The ocean dynamical thermostat on 10- to 20-year time scales acts to strengthen the zonal SST gradient as warm surface waters pile up in the western basin while cold water continually upwells in the eastern basin (*13*). This mechanism is confirmed as a transient response to radiative forcing in coupled climate models (*14*). As extratropical waters warm and/or oceanic subtropical cells weaken, there is a progressive reduction in the supply of cold water to equatorial upwelling (*15*), causing the tropical Pacific to transition from an initial increase to a long-term decrease in zonal SST gradient (*14*, *16*). As the zonal SST gradient and the Walker circulation strength are coupled via the Bjerknes feedback, the Walker circulation also transitions from a fast strengthening response to a slow weakening response (*17*). A strengthening of zonal SST gradient (i.e., a La Niña–like pattern) is also remotely contributed by the Atlantic and Indian oceans warming through atmospheric teleconnections and the Bjerknes feedback (*18*–*20*). The zonal SST gradient strengthening in coupled climate models is absent in slab ocean models (SOMs), suggesting a critical role of the ocean dynamic effect for the initial response (*14*). Other mechanisms that do not involve ocean dynamic adjustments are proposed to explain the long-term reduction in zonal SST gradient (i.e., an El Niño–like pattern), including the slowdown of convective overturning associated with weaker radiative cooling relative to water vapor increase (*21*), strong evaporative damping rate over the warm pool (*22*), and low cloud feedbacks (*23*). Apart from these tropics-mediated mechanisms, the radiatively forced extratropical climate change effects can further modulate the tropical Pacific warming pattern (*24*). For example, Arctic and Antarctic sea ice losses lead to a more enhanced warming in the eastern than the western equatorial Pacific with reduced zonal SST gradient (*25*, *26*). This effect, however, is muted during the initial period because of Southern Ocean heat uptake that favors a La Niña–like cooling (*24*, *27*).

Together, the interactions between different mechanisms acting on distinct time scales lead to large uncertainties in the equatorial Pacific warming pattern (*14*). Here, we propose a modeling approach to explicitly quantify the relative contribution of different mechanisms. Briefly, we reconstruct the near-future climate response to an abrupt CO_2 doubling in a fully coupled model (FULL) using a series of SOM experiments in which (i) the CO_2 concentrations are doubled with no other changes (SOM_CO2), (ii) sea ice fraction/thickness changes in FULL are prescribed in isolation (SOM_ICE), and (iii) net surface heat flux changes in FULL is prescribed separately over three different ocean basins—subpolar North Atlantic (SOM_NA), Southern Ocean (SOM_SO), and the

[1]Department of Urban and Environmental Engineering, Ulsan National Institute of Science and Technology, Ulsan 44919, Republic of Korea. [2]Division of Environmental Science and Engineering, Pohang University of Science and Technology (POSTECH), Pohang 37673, Republic of Korea. [3]Department of Earth and Atmospheric Sciences, Cornell University, Ithaca, NY, USA. [4]Scripps Institution of Oceanography, University of California San Diego, La Jolla, CA, USA. [5]Division of Earth and Climate Sciences, Nicholas School of the Environment, Duke University, Durham, NC, USA.
*Corresponding author. Email: skang@unist.ac.kr (S.M.K.); yechul.ycshin@gmail.com (Y.S.)

rest of the ocean (SOM_rest) (Materials and Methods). Separation of the effect of net surface heat flux changes from the CO_2 forcing and sea ice changes may seem arbitrary as they can affect the climate system through ocean dynamics. However, our aim is to isolate the role of net surface heat flux changes over the Southern Ocean and the subpolar North Atlantic, which are certain to cause surface cooling in a transient stage following CO_2 increase (Materials and Methods). To examine the linearity, we additionally conduct a SOM experiment in which changes in all of the aforementioned factors (e.g., CO_2 concentrations, sea ice cover changes, and global ocean heat uptake changes) are prescribed (SOM_ALL). We choose to examine the FULL response between 21 and 70 years after a CO_2 doubling because of the relevance to projected changes in the near future, with a focus on the equatorial Pacific warming pattern and the Walker circulation response.

Our idealized experimental setting reveals that a strengthening of zonal SST gradient and Walker circulation results from the Southern Ocean heat uptake while all other forcing agents cause it to weaken. We further show that the extent to which the Southern Ocean takes up heat explains a large portion of the inter-model discrepancies in the tropical warming pattern and the Walker circulation response in Coupled Model Intercomparison Project phase 6 (CMIP6) abrupt-4xCO2 experiments. Distinct from the prevailing notion whereby an ocean thermostat explains an initial strengthening of the zonal SST gradient, we propose an alternative mechanism in which the Southern Ocean heat uptake controls the tropical Pacific warming and circulation pattern primarily via atmospheric teleconnections.

RESULTS

Decomposition of tropical Pacific climate response pattern

The FULL experiment features polar amplification (Fig. 1A), El Niño–like warming (Fig. 1D), and the Walker circulation weakening (Fig. 1G). A key quantity to the surface warming pattern formation is the net surface heat flux Q_{net}, as the SSTs are intrinsically determined by the net surface heat budget. Hence, the slab ocean forced with global Q_{net} changes diagnosed from FULL can successfully reconstruct the FULL response when the same CO_2 radiative forcing and sea ice fraction/thickness changes are prescribed (contrast left and middle columns of Fig. 1). Specifically, the response patterns of SST and Walker circulation in SOM_ALL are starkly similar to those in FULL, with the pattern correlation of 0.98 in terms of global SST changes (Fig. 1, A and B). We note that the climate response patterns in FULL and, hence, SOM_ALL well represent the multimodel mean (MMM) response of CMIP6 CO_2 quadrupling experiments (fig. S1). The SST responses in FULL and CMIP6 MMM are strongly correlated at 0.95 globally and at 0.65 between 30°S and 30°N. Moreover, net surface heat flux Q_{net} changes exhibit a broad similarity between FULL and CMIP6 MMM (r = 0.57; fig. S1, C and D), with pronounced ocean heat uptake in the subpolar North Atlantic and the Southern Ocean. Thus, we expect that the decomposition results presented below will be largely valid in other CMIP6 models.

The SOM_ALL response is, in turn, well approximated by the sum of individual SOM experiments (SOM_SUM; contrast middle and right columns of Fig. 1). The tropical SST responses share strong spatial similarities between SOM_ALL and SOM_SUM with a pattern correlation of 0.84 between 30°S and 30°N. As a result, the climate response patterns in SOM_SUM resemble those in FULL (contrast left and right columns of Fig. 1); the pattern correlation of tropical SST response is 0.54. Spatial similarity between FULL, SOM_ALL, and SOM_SUM is also seen in the Walker circulation response (Fig. 1, G to I). This spatial linearity is a key result as it suggests that we may diagnostically use the SOM experiments to decompose the CO_2-driven FULL near-future response into the contributions from thermodynamic CO_2 radiative effect, sea ice changes, and regional ocean heat uptake changes.

We use individual SOM experiments to identify the factors that drive the El Niño–like warming and the Walker circulation slowdown in FULL. A reduction in the zonal SST gradient results from reduced sea ice extent (SOM_ICE) and local ocean heat uptake (SOM_rest), which is substantially offset by the Southern Ocean heat uptake (SOM_SO), with little contribution from the CO_2 radiative forcing (SOM_CO2) and the North Atlantic heat uptake (SOM_NA) (Fig. 1J). Notably, changes in the zonal SST gradient poorly explain changes in the Walker circulation strength in SOM_CO2 (Fig. 1, J and K). In contrast to the minimal effect on the zonal SST gradient, SOM_CO2 contributes most to a weakening of the Walker circulation (Fig. 1K). This is consistent with previous studies that demonstrate that the Walker circulation weakening is caused primarily by the uniform SST warming rather than the pattern of SST warming (*28*, *29*).

Atmosphere-mediated mechanisms

We first examine the contribution from the atmosphere-mediated mechanisms, namely, SOM_CO2 and SOM_ICE. The tropical-wide warming is primarily caused by SOM_CO2, accompanied by a large increase in tropospheric stability following the moist adiabatic adjustment (fig. S2) (*30*), effectively weakening the Walker circulation (Fig. 1K) (*28*, *29*). While SOM_CO2 induces the strongest equatorial warming (Fig. 2B), it exhibits a minimal zonal structure along the Pacific (Fig. 2G). This is in stark contrast to previous SOM experiments that exhibit a clear zonal gradient reduction in response to enhanced CO_2 concentrations (*2*, *31*). This has been explained by less-efficient evaporative cooling over the climatologically cold eastern Pacific than over the climatologically warm western Pacific. The evaporative damping mechanism is at work in our SOM_CO2 (Fig. 3D), as can be seen from the so-called curvature term, which quantifies the effect of zonal contrast in evaporative damping term in the surface energy budget (Materials and Methods). However, the enhanced East Pacific warming from the evaporative damping mechanism is overcompensated by negative shortwave cloud radiative effect localized over the eastern equatorial Pacific (Fig. 3C), as a consequence of the increase in low cloud cover because of enhanced tropospheric static stability (fig. S2B). The low cloud cover increase can be found in other previous SOM experiments under a CO_2 doubling [see Fig. 5A in (*23*)]. While the cloud radiative response is likely highly model dependent (*32*), our results suggest that the direct CO_2 effect is not so effective at producing zonal structures in the equatorial Pacific SST changes in the absence of sea ice changes.

We suggest that the CO_2-induced zonal SST contrast weakening in previous SOM experiments, which commonly include an interactive sea ice model, is partially due to the effect of sea ice loss, as the sum of SOM_CO2 and SOM_ICE indicates a clear gradient weakening (Fig. 1J). In particular, the Antarctic sea ice loss is critical for zonal temperature gradient weakening as the southern high-latitude

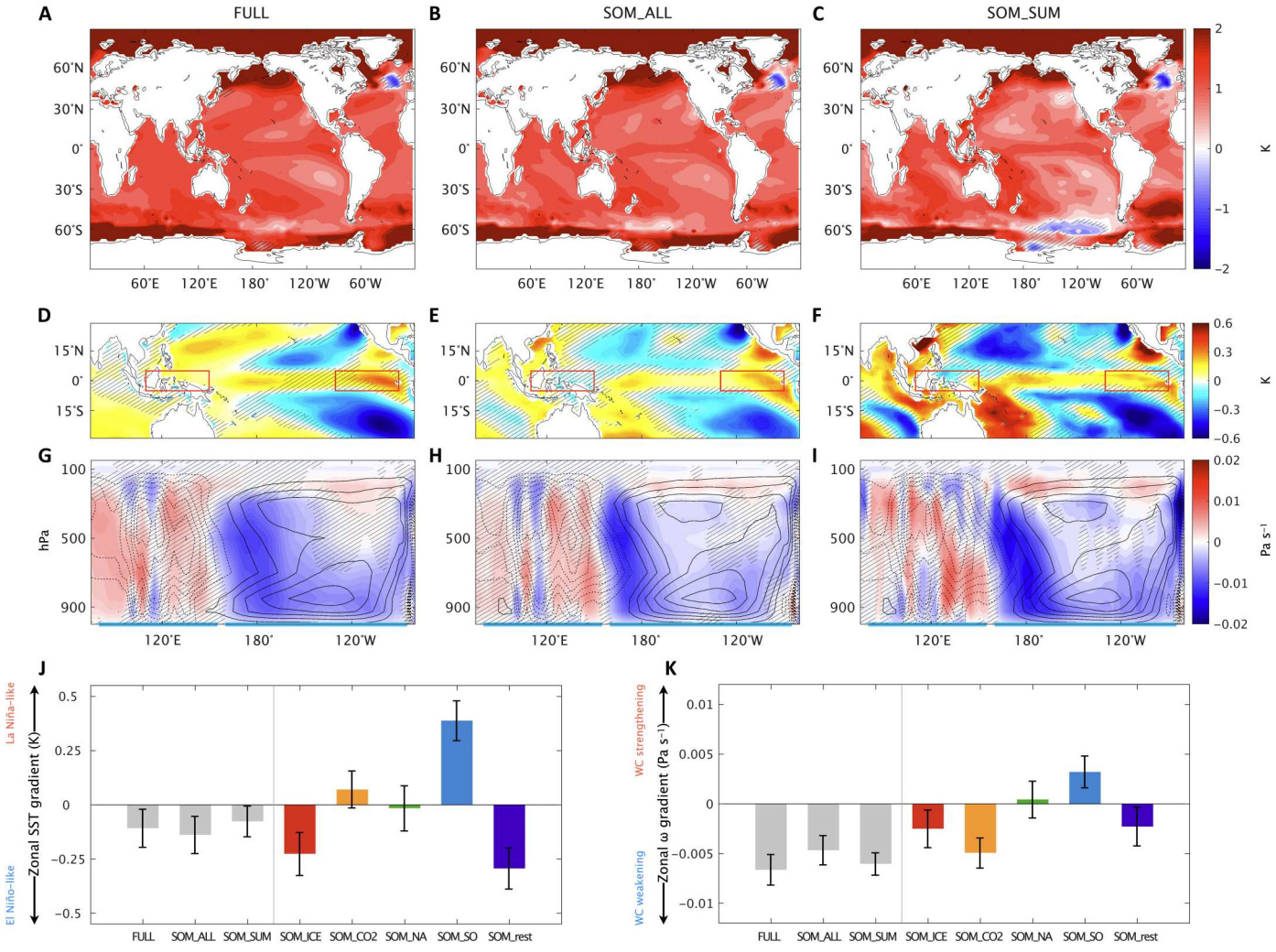

Fig. 1. Linearity of climate response. (**A** to **C**) Global SST response, (**D** to **F**) SST response relative to the tropical Pacific (30°S to 30°N, 75°E to 100°W) mean, and (**G** to **I**) equatorial Pacific pressure velocity response (shading) with the control climatology overlaid in contours (dashed, ascending; solid, descending; interval of 0.007 Pa s^{-1}) in FULL (left), SOM_ALL (middle), and SOM_SUM (right). The regions with the response insignificant at 95% confidence level based on the two-sided *t* test are hatched. (**J**) Difference in SST response between the two red boxes indicated in (D) to (F), a measure of the zonal SST gradient response in the equatorial Pacific. (**K**) Difference in 500-hPa pressure velocity response between the climatological descent and ascent regions, indicated by thick cyan lines in (G) to (I), a measure of the Walker circulation strength response. WC, Walker circulation.

effect reaches the equatorial Pacific through the eastern basin, whereas the northern high-latitude effect extends into the central equatorial Pacific owing to the climatological Intertropical Convergence Zone (ITCZ) blocking effect (*24*, *33*). In SOM_ICE (Fig. 2, A and F), high-latitude warming effects from sea ice loss propagate equatorward via wind-evaporation-SST (WES) feedback, which are further amplified by positive shortwave cloud radiative feedback (Fig. 3, A and B) (*34*, *35*). Thus, our experimental setting allows us to gain insight into the central role of sea ice loss in the El Niño–like warming pattern, more so than the direct CO_2 forcing itself. The Walker circulation weakens in SOM_ICE, albeit by a smaller extent than in SOM_CO2 (Fig. 1K).

Ocean-mediated mechanisms

We now move to discuss the ocean-mediated mechanisms, namely, SOM_NA, SOM_SO, and SOM_rest. Ocean heat uptake pattern plays a key role in the surface warming pattern formation (*36*). In particular, the Southern Ocean and the North Atlantic take up a great amount of heat because of increased CO_2 from the atmosphere (fig. S1, C and D) (*37*). The upwelling of pristine deep water makes the Southern Ocean an effective region of heat uptake (*38*), whereas the North Atlantic heat uptake is a result of the weakened Atlantic Meridional Overturning Circulation (*39*). For the time period we are investigating, the Southern Ocean and the North Atlantic take up a comparable amount of heat of 0.2 PW but the accompanying climate response is distinct in amplitude and spatial pattern. The SOM_NA is characterized by a prominent interhemispheric contrast, with a locally amplified and widespread cooling confined to the Northern Hemisphere (Fig. 2C), associated with the ITCZ blocking effect (*24*, *33*). In contrast to the strong north-south gradient, the tropical Pacific SST response shows little east-west gradient (Figs. 1J and 2H) (*35*, *40*). The Walker circulation change, hence,

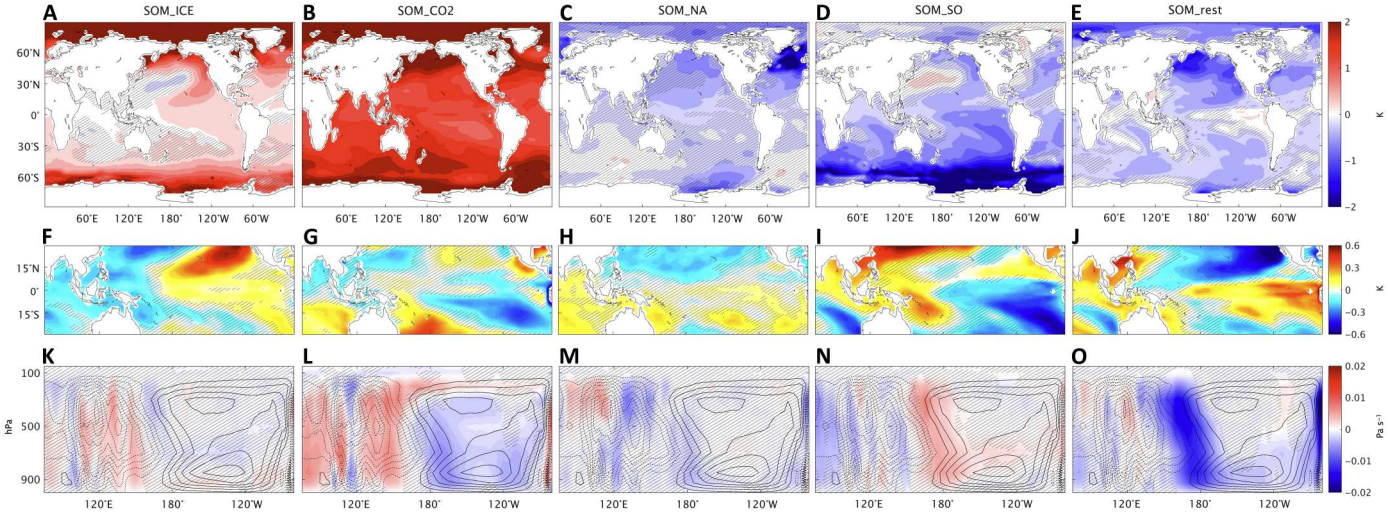

Fig. 2. Decomposition of climate response. (**A** to **E**) Global SST response, (**F** to **J**) SST response relative to the tropical Pacific (30°S to 30°N, 75°E to 100°W) mean, and (**K** to **O**) equatorial Pacific pressure velocity response (shading) with the control climatology overlaid in contours (dashed, ascending; solid, descending; interval of 0.007 Pa s^{-1}) in SOM_ICE, SOM_CO2, SOM_NA, SOM_SO, and SOM_rest. The regions with the response insignificant at 95% confidence level based on the two-sided *t* test are hatched.

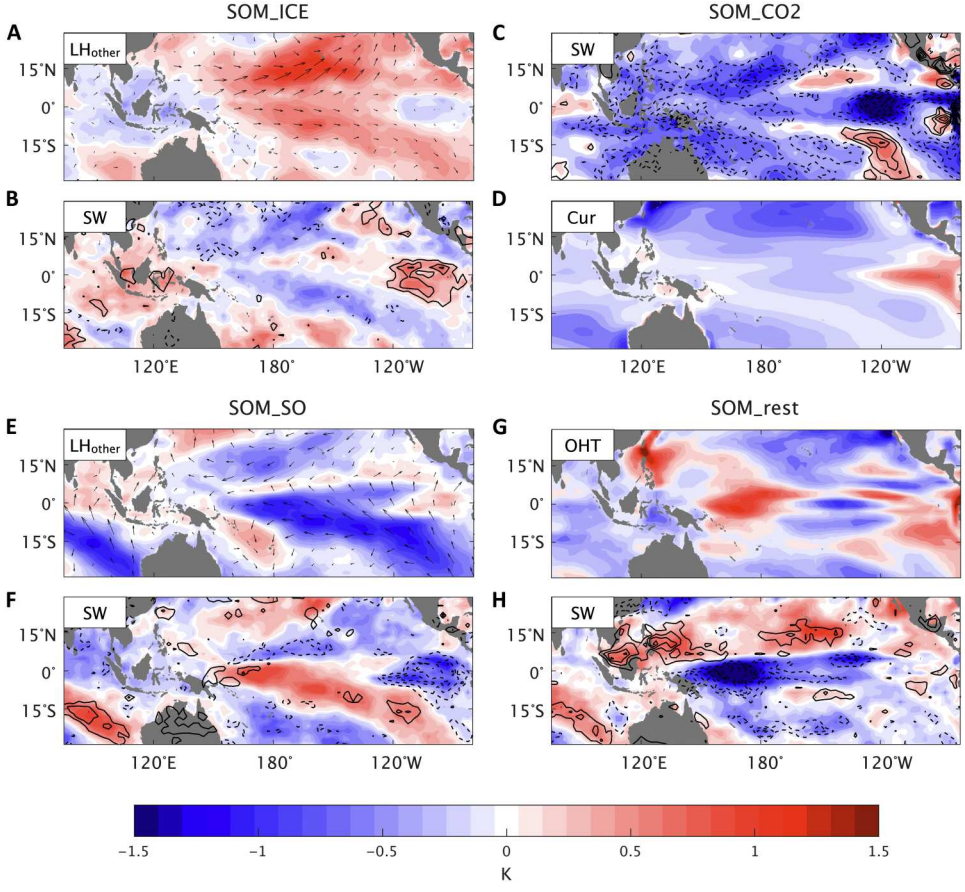

Fig. 3. Two dominant mechanisms for SST response. SST changes due to (**A**) latent heat flux changes resulting from wind anomalies (LH_{other}; shading) and 10-m wind anomaly vectors, as well as (**B**) net surface shortwave flux changes (SW; shading) and that due to low cloud changes (SW_{low}; downward in solid and upward in dashed contours; interval of 1.5 W m^{-2}; Materials and Methods) for SOM_ICE, (**C**) SW (shading) and SW_{low} (contours), and (**D**) the effect of zonal contrast in evaporative damping term (curvature; Materials and Methods) for SOM_CO2, (**E**) LH_{other} (shading) and 10-m wind anomaly vectors, and (**F**) SW (shading) and SW_{low} (contours) for SOM_SO, (**G**) prescribed Q_{net}, and (**H**) SW (shading) and SW_{low} (contours) for SOM_rest.

is negligible in SOM_NA (Figs. 1K and 2M). By contrast, SOM_SO shows the surface cooling response penetrating across the equator through the East Pacific (Fig. 2D), giving rise to a clear La Niña–like pattern (Fig. 2I) (*24*) and consequently a strongly enhanced zonal SST gradient (Fig. 1J) and Walker circulation (Figs. 1K and 2N). The equatorward propagation of the Southern Ocean cooling effect is enabled primarily via WES feedback (Fig. 3E), which is enhanced by the shortwave cloud feedback in the southeastern Pacific (Fig. 3F) (*34*, *35*). The La Niña–like cooling in SOM_SO intensifies the northeasterlies in the subtropical North Pacific (Fig. 3E), thereby extending the cooling response into the opposite hemisphere (Fig. 2D). This is distinct from SOM_NA, wherein the SST response is limited to the forcing hemisphere (Fig. 2C). As a consequence, the global SST cooling response is nearly three times larger in SOM_SO than in SOM_NA (−0.52 K versus −0.19 K).

In SOM_rest, there is overall cooling in the extratropics and warming in the eastern equatorial Pacific (Fig. 2E), as ocean heat uptake is largely positive (i.e., downward net surface heat flux anomaly) in the extratropics and weakly negative (i.e., upward net surface heat flux anomaly) near the equator (fig. S1, C and D), primarily because of ocean circulation changes (*41*). Anomalous ocean heat flux convergence is prescribed in both the western and eastern equatorial Pacific (Fig. 3G), but its effect in the western basin is offset by a negative shortwave cloud radiative effect (Fig. 3H) as a result of locally enhanced deep convection (fig. S2E). As a result, SOM_rest induces a clear El Niño–like pattern (Fig. 2J) with a weakened and eastward-shifted Walker circulation (Figs. 1K and 2O).

DISCUSSION

We have investigated the tropical Pacific response to increased CO_2 using a SOM as a diagnostic modeling tool, which isolates the direct effect of CO_2 forcing from polar sea ice loss and regional ocean heat uptake. This diagnostic tool successfully identifies important factors for the tropical Pacific warming pattern (i.e., El Niño–like warming) and the Walker circulation slowdown. It is found that the El Niño–like warming primarily results from Antarctic ice loss and local ocean heat uptake response with a negligible contribution from the direct CO_2 effect. The Antarctic sea ice loss has been previously shown to reduce the zonal gradient of the tropical Pacific SST, but its importance relative to other CO_2-induced climatic effects has not been assessed. Here, we demonstrate the central role of sea-ice loss in the equatorial Pacific warming pattern, resulting in a considerable slowdown of the Walker circulation. However, the CO_2 forcing contributes predominantly to the Walker circulation slowdown by enhancing the tropical tropospheric stability, despite a minimal effect on the zonal SST pattern over the equatorial Pacific. The local net surface heat flux response, upward from the western and eastern equatorial Pacific, also contributes to weakening the zonal SST gradient and the Walker circulation.

Our idealized experiment setup reveals that the El Niño–like warming and the Walker circulation slowdown are considerably compensated by the effect of the Southern Ocean heat uptake. The heat uptake in the subpolar North Atlantic, comparable in magnitude to that over the Southern Ocean, has little impact on tropical Pacific climate. The critical role of the Southern Ocean for the tropical Pacific climate response is further corroborated by the CMIP6 inter-model regression analysis: The extent to which the Southern Ocean takes up heat explains a considerable fraction of the inter-model spread in the tropical Pacific climate response to quadrupled CO_2 concentrations (Fig. 4). Specifically, we regress the global SST and the equatorial Pacific omega responses onto Q_{net} changes averaged between 40°S and 70°S. The inter-model regression patterns are consistent with the Southern Ocean–induced teleconnection pattern in SOM_SO (contrast Fig. 2, D and N, with Fig. 4, A and B). The models with a larger Southern Ocean heat uptake are associated with a greater La Niña–like cooling ($r = 0.66$; $P < 0.01$) (Fig. 4C) and a stronger Walker circulation intensification ($r = 0.39$; $P < 0.05$) (Fig. 4D). Thus, our results suggest that an initial strengthening of equatorial Pacific SST gradient and Walker circulation may be a result of Southern Ocean heat uptake via atmospheric teleconnections.

Our study has important implications for the well-known discrepancy between the coupled climate model simulations and observations in terms of the recent Pacific SST trend patterns. The eastern equatorial Pacific and the Southern Ocean are simulated to have warmed in the recent historical period while they are observed to have significantly cooled (*42*). Our results suggest that the model observation discrepancy in the tropical Pacific SST trends may be partly attributable to missing cooling trends over the Southern Ocean, for example, because of the absence of Antarctic meltwater discharge in model simulations (*43*), biased Southern Ocean clouds (*44*), inability to simulate natural decadal variability of Southern Ocean SST (*45*, *46*), and misrepresentation of Antarctic ozone hole effects (*47*). On centennial and longer time scales, the Southern Ocean heat uptake gradually weakens as a result of slow but steady SST increase. Our SOM_SO suggests that the Southern Ocean warming on the long time scales will turn to contribute to an El Niño–like warming and the Walker circulation slowdown. This effect, however, will be counteracted by the Southern Ocean cooling induced by Antarctic meltwater (*48*), to the extent that is uncertain. Our results point to the importance of constraining the Southern Ocean heat uptake to bridge the gap between the simulated and observed SST trends and to narrow the uncertainty in projecting tropical Pacific climate pattern.

MATERIALS AND METHODS

Model and experiment

We use the National Center for Atmospheric Research (NCAR) Community Earth System Model (CESM) version 1.2.2 (*49*) with the Community Atmosphere Model version 4 (CAM4) (*50*). Atmosphere and land models consist of a nominal 2° horizontal resolution with 26 vertical layers, and ocean and ice models have a nominal 1° horizontal resolution with 60 vertical layers for the ocean. The CAM4 is an older version in the NCAR family of atmospheric models, but it remains a useful tool, particularly for exploring dynamical mechanisms (*36*, *51*). Our proposed mechanism works well in explaining the inter-model spread of the state-of-the-art CMIP6 models (Fig. 4).

We first integrate two fully coupled experiments: the control run under preindustrial conditions and the perturbed run under abruptly doubled CO_2 concentrations. Both experiments are initialized from the end of a quasi-equilibrated preindustrial run of 900 years. The control climatology is obtained as the last 100-year average of the 140-year integration (FULL_CTL). The doubling CO_2 experiment is integrated for 70 years, and the last 50-year

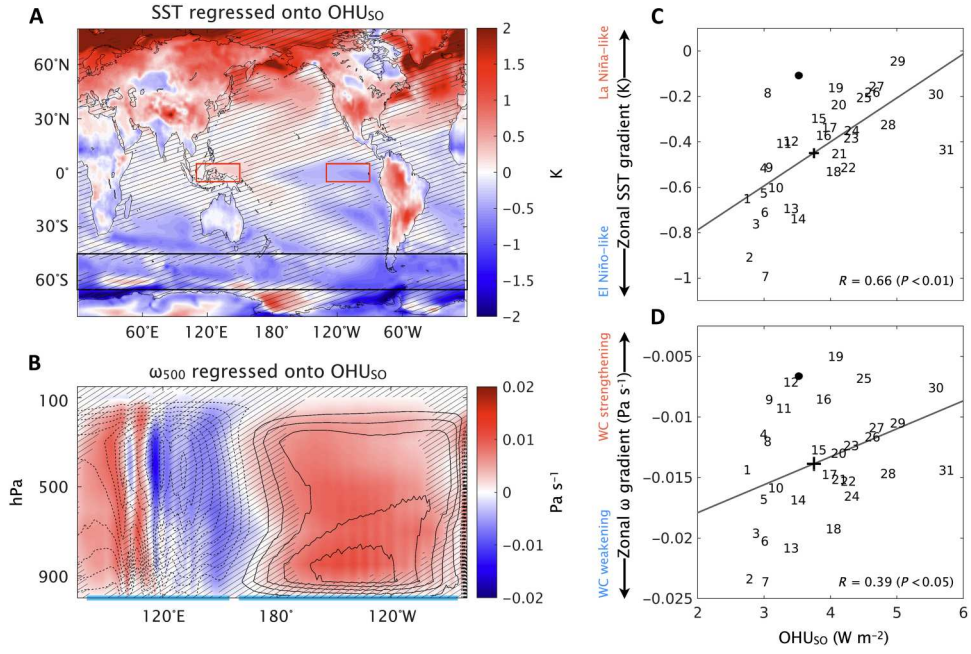

Fig. 4. CMIP6 inter-model regression. (**A**) Global mean removed SST response and (**B**) equatorial Pacific pressure velocity response, regressed onto Q_{net} changes averaged between 45°S and 65°S (OHU_{SO}) for 31 CMIP6 abrupt-4xCO2 simulations (model lists in table S1). The regression coefficients are multiplied by two inter-model SDs of Q_{net} changes to represent the inter-model discrepancies. The regions with the response insignificant at 95% confidence level based on the two-sided *t* test are hatched. Scatterplot of OHU_{SO} against (**C**) the equatorial Pacific zonal SST gradient and (**D**) the Walker circulation index. Models are numbered in the ascending order of the amplitude of Southern Ocean heat uptake. The plus symbol indicates the CMIP6 MMM and the black closed circle indicates our FULL response. The comparison is made by simply halving the CMIP6 responses between 21 and 70 years after an abruptly quadrupled CO_2 as our FULL experiment is forced by a CO_2 doubling.

average is used (FULL_2xCO2). We take the years 21 to 70 for our analysis to represent the near-future transient response to CO_2 forcing (*15*). The difference between FULL_2xCO2 and FULL_CTL is referred to as FULL.

To reconstruct the FULL response using the SOM, we integrate the SOM with the CO_2 concentrations, *Q* fluxes (i.e., net upward surface heat fluxes), and the ice fraction/thickness diagnosed from either FULL_2xCO2 or FULL_CTL, which respectively is denoted as SOM_2xCO2 and SOM_CTL. The difference between SOM_2xCO2 and SOM_CTL is referred to as SOM_ALL. We then conduct a series of SOM experiments that allows us to decompose the radiatively forced climate response into the contributions from direct CO_2 forcing, regional ocean heat uptake effect (*Q*), and ice fraction/thickness changes (ice), similar to the strategy in (*36*)

$$\underbrace{\delta X}_{\substack{\text{fully coupled}\\ \text{response}}} \approx \underbrace{f(\delta CO_2, \delta ice, \delta Q)}_{\text{SOM\_ALL}} \approx \underbrace{f(\delta CO_2, ice_c, Q_c)}_{\text{SOM\_CO2}} + \underbrace{f(CO_2, \delta ice, Q_c)}_{\text{SOM\_ICE}} + \underbrace{\sum f(CO_2, ice_c, \delta Q)}_{\text{SOM\_Qflux}} \quad (1)$$

where δ indicates the difference between the doubled CO_2 and the control experiments and the subscript *c* denotes the control climate state. Equation 1 states that any responses in the fully coupled model *X* can be diagnostically reconstructed using the SOM by prescribing CO_2 forcing, as well as changes in ice and *Q* fluxes, as in SOM_ALL. This can be confirmed by comparing the first (FULL) and second (SOM_ALL) columns of Fig. 1. A series of SOM experiments with prescribed changes in one factor at a time while fixing other factors to the control state will allow us to disentangle the individual contributions. For example, the effect of direct CO_2 forcing is estimated as the difference from SOM_CTL of the SOM experiment forced with doubled CO_2 concentrations and ice fraction/thickness and *Q* fluxes diagnosed from FULL_CTL (i.e., SOM_CO2). Similarly, the effect of ice changes is estimated as the difference from SOM_CTL of the SOM experiment forced with ice fraction/thickness from FULL_2xCO2 and CO_2 concentrations and *Q* fluxes from FULL_CTL (i.e., SOM_ICE). While there are multiple ways to incorporate the effect of sea ice loss in climate models (*52*), we apply the method of directly nudging anomalous ice properties. We estimate the ocean heat uptake effect separately for the North Atlantic (40°N to 75°N and 290°E to 0°E; SOM_NA), the Southern Ocean (65°S to 40°S; SOM_SO), and the rest of ocean area (SOM_rest), given that the North Atlantic and Southern Ocean are the two major regions of ocean heat uptake under global warming. All SOM experiments are integrated for 50 years, and the last 30-year average is analyzed.

We note that our experiment design cannot point to the origin of *Q* flux changes, which are the result of dynamical air-sea coupling as a response to different forcing agents. For example, ocean heat flux convergence anomaly in the Southeast Pacific may be a result of ocean circulation changes because of Southern Ocean heat uptake (*34*). Similarly, ocean heat flux divergence anomaly in the subtropical North Pacific may be a result of weakened subtropical cells in response to Arctic sea ice loss (*26*). In addition, ocean heat flux divergence anomaly in the subpolar North Atlantic may have partially resulted from Arctic sea ice loss that causes the Atlantic Meridional Overturning Circulation to weaken. That is, all forcing agents would

imprint onto the global ocean heat uptake. We consider these effects of ocean adjustment in a diagnostic framework by prescribing Q flux changes in FULL to SOM. While details of Q flux changes are not well constrained and suffer large inter-model spread, it is certain that anomalous ocean heat flux divergence occurs over the Southern Ocean and the subpolar North Atlantic in a transient stage following CO_2 increase. This is why we isolate the role of Q flux changes over those two regions (SOM_SO and SOM_NA) from the rest of the ocean (SOM_rest). We note that the choice of decomposition is somewhat arbitrary and subjective, but our aim is to disentangle the CO_2-induced effects with high confidence, such as polar ice melt, Southern Ocean heat uptake, and the North Atlantic warm hole. We believe that this diagnostic approach offers useful insights to understanding the global warming pattern formation.

SST decomposition using surface energy budget

The causes of the SST responses can be understood based on the surface energy budget (*2*). Assuming a steady-state ocean mixed layer, the changes in heat budget for the ocean mixed layer is

$$0 = \delta\mathrm{SW} + \delta\mathrm{LW} - \delta\mathrm{LH} - \delta\mathrm{SH} + \delta\mathrm{OHT} \quad (2)$$

where SW is net downward surface shortwave flux, LW is net downward surface longwave flux, LH is upward latent heat flux, and SH is upward sensible heat flux. The OHT represents the convergence of ocean heat transport for fully coupled experiments, which is prescribed to mimic the ocean heat uptake effect for slab-coupled experiments. To associate the surface flux responses with the surface temperature T_s, we separate the component because of the surface temperature changes from δLH (*53*, *54*)

$$\delta\mathrm{LH} = \left(\frac{\partial \mathrm{LH}}{\partial T_s}\right)\delta T_s + \delta\mathrm{LH}_{\mathrm{others}} = (\alpha\overline{\mathrm{LH}})\delta T_s + \delta\mathrm{LH}_{\mathrm{others}} \quad (3)$$

where the overbar denotes the reference climate state and $\alpha = L_v/(R_v\overline{T_s}^2)$ with the latent heat of vaporization $L_v = 2.5 \times 10^6$ J kg^{-1} and $R_v = 461.5$ J kg^{-1}K^{-1}. $\delta\mathrm{LH}_{\mathrm{others}}$ indicates the LH changes due to the factors other than SST changes, which primarily results from surface wind speed changes (*55*). Substituting Eq. 3 into Eq. 2 allows us to decompose the SST responses into contributions from individual surface heat flux components

$$\delta T_s = \frac{\delta\mathrm{SW} + \delta\mathrm{LW} - \delta\mathrm{LH}_{\mathrm{others}} - \delta\mathrm{SH} + \delta\mathrm{OHT}}{\alpha\overline{\mathrm{LH}}} \quad (4)$$

Note that the denominator of Eq. 4, $\frac{\partial \mathrm{LH}}{\partial T_s}$, indicates the degree of LH change per unit SST increase, which infers the evaporative damping efficiency in the reference climate. Because of the Clausius-Clapeyron relation, the evaporative damping efficiency is larger over the climatologically warmer western Pacific than the climatologically colder eastern Pacific. We separate out the effect of zonal contrast in evaporative damping efficiency by reformulating Eq. 4 following Park *et al.* (*55*)

$$\delta T_s = \underbrace{\frac{\mathrm{num}}{[-\alpha\overline{\mathrm{LH}}]}}_{\substack{\text{contribution of each}\\ \text{surface flux component}}} + \underbrace{\left(\frac{\mathrm{num}}{-\alpha\overline{\mathrm{LH}}} - \frac{\mathrm{num}}{[-\alpha\overline{\mathrm{LH}}]}\right)}_{\substack{\text{contribution of curvature in}\\ \text{evaporative damping efficiency}}} \quad (5)$$

where num is the numerator of Eq. 4 and brackets indicate the zonal average. In sum, the surface temperature response can be decomposed into six components

$$\delta T_s = \delta T_{\mathrm{SW}} + \delta T_{\mathrm{LW}} + \delta T_{\mathrm{LH}_{\mathrm{others}}} + \delta T_{\mathrm{SH}} + \delta T_{\mathrm{OHT}} + \delta T_{\mathrm{curvature}} \quad (6)$$

Figure 3 shows the two major components in Eq. 6 for individual SOM experiments. Note that shortwave flux changes are further attributed to low cloud changes, assuming that cloud radiative effects are dominated by low clouds when the absolute ratio of the longwave to the shortwave cloud radiative effect is smaller than 0.41 (*56*). Cloud radiative effects are calculated by subtracting clear sky from all sky radiative components.

Supplementary Materials

This PDF file includes:

Figs. S1 and S2
Table S1

REFERENCES AND NOTES

1. S. Manabe, R. J. Stouffer, Sensitivity of a global climate model to an increase of CO2concentration in the atmosphere. *J. Geophys. Res. Oceans.* **85**, 5529–5554 (1980).
2. S.-P. Xie, C. Deser, G. A. Vecchi, J. Ma, H. Teng, A. T. Wittenberg, Global warming pattern formation: Sea surface temperature and rainfall. *J. Climate* **23**, 966–986 (2010).
3. M. R. Grose, J. Bhend, S. Narsey, A. S. Gupta, J. R. Brown, Can we constrain CMIP5 rainfall projections in the tropical pacific based on surface warming patterns? *J. Climate* **27**, 9123–9138 (2014).
4. K. E. Trenberth, G. W. Branstator, D. Karoly, A. Kumar, N.-C. Lau, C. Ropelewski, Progress during TOGA in understanding and modeling global teleconnections associated with tropical sea surface temperatures. *J. Geophys. Res. Oceans* **103**, 14291–14324 (1998).
5. J. Choi, S.-I. An, J.-S. Kug, S.-W. Yeh, The role of mean state on changes in El Niño's flavor. *Climate Dyn.* **37**, 1205–1215 (2011).
6. P. N. DiNezio, B. P. Kirtman, A. C. Clement, S.-K. Lee, G. A. Vecchi, A. Wittenberg, Mean climate controls on the simulated response of ENSO to increasing greenhouse gases. *J. Climate* **25**, 7399–7420 (2012).
7. G. Wang, W. Cai, A. Santoso, L. Wu, J. C. Fyfe, S.-W. Yeh, B. Ng, K. Yang, M. J. McPhaden, Future Southern Ocean warming linked to projected ENSO variability. *Nat. Clim. Chang.* **12**, 649–654 (2022).
8. Y.-M. Yang, J.-H. Park, S.-I. An, B. Wang, X. Luo, Mean sea surface temperature changes influence ENSO-related precipitation changes in the mid-latitudes. *Nat. Commun.* **12**, 1495 (2021).
9. C. Zhou, M. D. Zelinka, S. A. Klein, Impact of decadal cloud variations on the Earth's energy budget. *Nat. Geosci.* **9**, 871–874 (2016).
10. P. Ceppi, J. M. Gregory, Relationship of tropospheric stability to climate sensitivity and Earth's observed radiation budget. *Proc. Natl. Acad. Sci. U.S.A.* **114**, 13126–13131 (2017).
11. T. Andrews, M. J. Webb, The dependence of global cloud and lapse rate feedbacks on the spatial structure of tropical pacific warming. *J. Climate* **31**, 641–654 (2018).
12. Y. Dong, K. C. Armour, M. D. Zelinka, C. Proistosescu, D. S. Battisti, C. Zhou, T. Andrews, Intermodel spread in the pattern effect and its contribution to climate sensitivity in CMIP5 and CMIP6 models. *J. Climate* **33**, 7755–7775 (2020).
13. A. C. Clement, R. Seager, M. A. Cane, S. E. Zebiak, An ocean dynamical thermostat. *J. Climate* **9**, 2190–2196 (1996).
14. U. K. Heede, A. V. Fedorov, N. J. Burls, Time scales and mechanisms for the tropical pacific response to global warming: A tug of war between the ocean thermostat and weaker walker. *J. Climate* **33**, 6101–6118 (2020).
15. M. F. Stuecker, A. Timmermann, F.-F. Jin, C. Proistosescu, S. M. Kang, D. Kim, K.-S. Yun, E.-S. Chung, J.-E. Chu, C. M. Bitz, K. C. Armour, M. Hayashi, Strong remote control of future equatorial warming by off-equatorial forcing. *Nat. Clim. Chang.* **10**, 124–129 (2020).
16. U. K. Heede, A. V. Fedorov, Eastern equatorial Pacific warming delayed by aerosols and thermostat response to CO_2 increase. *Nat. Clim. Chang.* **11**, 696–703 (2021).
17. K. Lu, J. He, B. Fosu, M. Rugenstein, Mechanisms of fast walker circulation responses to CO_2 forcing. *Geophys. Res. Lett.* **48**, e2021GL095708 (2021).
18. S. McGregor, A. Timmermann, M. F. Stuecker, M. H. England, M. Merrifield, F.-F. Jin, Y. Chikamoto, Recent walker circulation strengthening and Pacific cooling amplified by Atlantic warming. *Nat. Clim. Chang.* **4**, 888–892 (2014).

19. X. Li, S.-P. Xie, S. T. Gille, C. Yoo, Atlantic-induced pan-tropical climate change over the past three decades. *Nat. Clim. Chang.* **6**, 275–279 (2016).
20. B. Fosu, J. He, G. Liguori, Equatorial Pacific warming attenuated by SST warming patterns in the tropical Atlantic and Indian Oceans. *Geophys. Res. Lett.* **47**, e2020GL088231 (2020).
21. G. A. Vecchi, B. J. Soden, Global warming and the weakening of the tropical circulation. *J. Climate* **20**, 4316–4340 (2007).
22. S.-P. Xie, Ocean warming pattern effect on global and regional climate change. *AGU Adv.* **1**, e2019AV000130 (2020).
23. E. Erfani, N. J. Burls, The strength of low-cloud feedbacks and tropical climate: A CESM sensitivity study. *J. Climate* **32**, 2497–2516 (2019).
24. S. M. Kang, S.-P. Xie, Y. Shin, H. Kim, Y.-T. Hwang, M. F. Stuecker, B. Xiang, M. Hawcroft, Walker circulation response to extratropical radiative forcing. *Sci. Adv.* **6**, eabd3021 (2020).
25. C. Deser, R. A. Tomas, L. Sun, The role of ocean–atmosphere coupling in the zonal-mean atmospheric response to arctic sea ice loss. *J. Climate* **28**, 2168–2186 (2015).
26. M. R. England, L. M. Polvani, L. Sun, C. Deser, Tropical climate responses to projected Arctic and Antarctic sea-ice loss. *Nat. Geosci.* **13**, 275–281 (2020).
27. Y.-T. Hwang, S.-P. Xie, C. Deser, S. M. Kang, Connecting tropical climate change with Southern Ocean heat uptake. *Geophys. Res. Lett.* **44**, 9449–9457 (2017).
28. J. Ma, S.-P. Xie, Y. Kosaka, Mechanisms for tropical tropospheric circulation change in response to global warming. *J. Climate* **25**, 2979–2994 (2012).
29. J. He, B. J. Soden, Anthropogenic weakening of the tropical circulation: The relative roles of direct CO_2 forcing and sea surface temperature change. *J. Climate* **28**, 8728–8742 (2015).
30. T. R. Knutson, S. Manabe, Time-mean response over the tropical pacific to increased $C0_2$ in a coupled ocean-atmosphere model. *J. Climate* **8**, 2181–2199 (1995).
31. T. M. Merlis, T. Schneider, Changes in zonal surface temperature gradients and walker circulations in a wide range of climates. *J. Climate* **24**, 4757–4768 (2011).
32. B. J. Soden, I. M. Held, An assessment of climate feedbacks in coupled ocean–atmosphere models. *J. Climate* **19**, 3354–3360 (2006).
33. Y. Shin, S. M. Kang, How does the high-latitude thermal forcing in one hemisphere affect the other hemisphere? *Geophys. Res. Lett.* **48**, e2021GL095870 (2021).
34. H. Kim, S. M. Kang, J. E. Kay, S.-P. Xie, Subtropical clouds key to Southern Ocean teleconnections to the tropical Pacific. *Proc. Natl. Acad. Sci. U.S.A.* **119**, e2200514119 (2022).
35. W.-T. Hsiao, Y. T. Hwang, Y.-J. Chen, S. M. Kang, The role of clouds in shaping tropical pacific response pattern to extratropical thermal forcing. *Geophys. Res. Lett.* **49**, e2022GL098023 (2022).
36. S. Hu, S.-P. Xie, S. M. Kang, Global warming pattern formation: The role of ocean heat uptake. *J. Climate* **35**, 1885–1899 (2022).
37. J. Marshall, J. R. Scott, K. C. Armour, J.-M. Campin, M. Kelley, A. Romanou, The ocean's role in the transient response of climate to abrupt greenhouse gas forcing. *Climate Dyn.* **44**, 2287–2299 (2015).
38. K. C. Armour, J. Marshall, J. R. Scott, A. Donohoe, E. R. Newsom, Southern ocean warming delayed by circumpolar upwelling and equatorward transport. *Nat. Geosci.* **9**, 549–554 (2016).
39. M. Winton, S. M. Griffies, B. L. Samuels, J. L. Sarmiento, T. L. Frölicher, Connecting changing ocean circulation with changing climate. *J. Climate* **26**, 2268–2278 (2013).
40. S. M. Kang, K. Park, Y.-T. Hwang, W.-T. Hsiao, Contrasting tropical climate response pattern to localized thermal forcing over different ocean basins. *Geophys. Res. Lett.* **45**, 12544–12552 (2018).
41. S. Hu, S.-P. Xie, W. Liu, Global pattern formation of net ocean surface heat flux response to greenhouse warming. *J. Climate* **33**, 7503–7522 (2020).
42. R. C. J. Wills, Y. Dong, C. Proistosecu, K. C. Armour, D. S. Battisti, Systematic climate model biases in the large-scale patterns of recent sea-surface temperature and sea-level pressure change. *Geophys. Res. Lett.* **49**, e2022GL100011 (2022).
43. R. Bintanja, G. J. van Oldenborgh, S. S. Drijfhout, B. Wouters, C. A. Katsman, Important role for ocean warming and increased ice-shelf melt in Antarctic sea-ice expansion. *Nat. Geosci.* **6**, 376–379 (2013).
44. A. Bodas-Salcedo, K. D. Williams, M. A. Ringer, I. Beau, J. N. S. Cole, J.-L. Dufresne, T. Koshiro, B. Stevens, Z. Wang, T. Yokohata, Origins of the solar radiation biases over the southern ocean in CFMIP2 models. *J. Climate* **27**, 41–56 (2014).
45. M. Latif, T. Martin, W. Park, Southern ocean sector centennial climate variability and recent decadal trends. *J. Climate* **26**, 7767–7782 (2013).
46. L. Zhang, T. L. Delworth, W. Cooke, X. Yang, Natural variability of Southern Ocean convection as a driver of observed climate trends. *Nat. Clim. Chang.* **9**, 59–65 (2019).
47. D. L. Hartmann, The Antarctic ozone hole and the pattern effect on climate sensitivity. *Proc. Natl. Acad. Sci. U.S.A.* **119**, e2207889119 (2022).
48. B. Bronselaer, M. Winton, S. M. Griffies, W. J. Hurlin, K. B. Rodgers, O. V. Sergienko, R. J. Stouffer, J. L. Russell, Change in future climate due to Antarctic meltwater. *Nature* **564**, 53–58 (2018).
49. J. W. Hurrell, M. M. Holland, P. R. Gent, S. Ghan, J. E. Kay, P. J. Kushner, J.-F. Lamarque, W. G. Large, D. Lawrence, K. Lindsay, W. H. Lipscomb, M. C. Long, N. Mahowald, D. R. Marsh, R. B. Neale, P. Rasch, S. Vavrus, M. Vertenstein, D. Bader, W. D. Collins, J. J. Hack, J. Kiehl, S. Marshall, The community earth system model: A framework for collaborative research. *Bull. Am. Meteorol. Soc.* **94**, 1339–1360 (2013).
50. R. B. Neale, J. Richter, S. Park, P. H. Lauritzen, S. J. Vavrus, P. J. Rasch, M. Zhang, The mean climate of the community atmosphere model (CAM4) in Forced SST and fully coupled experiments. *J. Climate* **26**, 5150–5168 (2013).
51. D. Kim, H. Kim, S. M. Kang, M. F. Stuecker, T. M. Merlis, Weak Hadley cell intensity changes due to compensating effects of tropical and extratropical radiative forcing. *NPJ Clim. Atmos. Sci.* **5**, 61 (2022).
52. M. R. England, I. Eisenman, T. J. W. Wagner, Spurious climate impacts in coupled sea ice loss simulations. *J. Climate* **35**, 3801–3811 (2022).
53. F. Jia, L. Wu, A study of response of the equatorial pacific SST to doubled-CO_2 forcing in the coupled CAM–1.5-layer reduced-gravity ocean model. *J. Phys. Oceanogr.* **43**, 1288–1300 (2013).
54. L. Zhang, T. Li, A simple analytical model for understanding the formation of sea surface temperature patterns under global warming. *J. Climate* **27**, 8413–8421 (2014).
55. C. Park, S. M. Kang, M. F. Stuecker, F.-F. Jin, Distinct surface warming response over the western and eastern equatorial pacific to radiative forcing. *Geophys. Res. Lett.* **49**, e2021GL095829 (2022).
56. M. J. Webb, C. A. Senior, D. M. H. Sexton, W. J. Ingram, K. D. Williams, M. A. Ringer, B. J. McAvaney, R. Colman, B. J. Soden, R. Gudgel, T. Knutson, S. Emori, T. Ogura, Y. Tsushima, N. Andronova, B. Li, I. Musat, S. Bony, K. E. Taylor, On the contribution of local feedback mechanisms to the range of climate sensitivity in two GCM ensembles. *Climate Dyn.* **27**, 17–38 (2006).

Acknowledgments

Funding: S.M.K. and H.K. have been supported by the Research Program for the carbon cycle between oceans, land, and atmosphere of the National Research Foundation (NRF) funded by the Ministry of Science and ICT(NRF-2022M3I6A1090965); Y.S. by the postdoctoral research fellowship of POSTECH Initiative for fostering Unicorn of Research & Innovation (PIURI) project; and S.P.X. by the National Science Foundation (AGS 1934392). **Author contributions:** S.M.K., S.-P.X., Y.S., and S.H. conceived the study and designed the experiments. Y.S. performed the experiments. Y.S. and H.K. analyzed the model output and produced figures. All authors contributed to the discussion of the results and the writing of the manuscript. **Competing interests:** The authors declare that they have no competing interests. **Data and materials availability:** All data needed to evaluate the conclusions in the paper are present in the paper and/or the Supplementary Materials. The postprocessed data are uploaded in https://doi.org/10.5281/zenodo.7251165. All CMIP data used for this study are downloaded from Earth System Grid Federation (ESGF) data portal (https://esgf-node.llnl.gov/projects/cmip6/).

Submitted 26 October 2022
Accepted 5 April 2023
Published 10 May 2023
10.1126/sciadv.adf5059

ScienceAdvances

Disentangling the mechanisms of equatorial Pacific climate change

Sarah M. Kang, Yechul Shin, Hanjun Kim, Shang-Ping Xie, and Shineng Hu

Sci. Adv., **9** (19), eadf5059.
DOI: 10.1126/sciadv.adf5059

Science Advances (ISSN) is published by the American Association for the Advancement of Science. 1200 New York Avenue NW, Washington, DC 20005. The title *Science Advances* is a registered trademark of AAAS.